Non-muscle MYH10/myosin IIB recruits ESCRT-III to participate in autophagosome closure to maintain neuronal homeostasis

Autophagy

Autophagy

ISSN: (Print) (Online) Journal homepage: www.tandfonline.com/journals/kaup20

Non-muscle MYH10/myosin IIB recruits ESCRT-III to participate in autophagosome closure to maintain neuronal homeostasis

Yong-Woo Jun, Soojin Lee, Byung-Kwan Ban, Jin-A Lee & Fen-Biao Gao

To cite this article: Yong-Woo Jun, Soojin Lee, Byung-Kwan Ban, Jin-A Lee & Fen-Biao Gao (2023) Non-muscle MYH10/myosin IIB recruits ESCRT-III to participate in autophagosome closure to maintain neuronal homeostasis, Autophagy, 19:7, 2045-2061, DOI: 10.1080/15548627.2023.2169309

To link to this article: https://doi.org/10.1080/15548627.2023.2169309

AUTOPHAGY
2023, VOL. 19, NO. 7, 2045–2061
https://doi.org/10.1080/15548627.2023.2169309

Taylor & Francis
Taylor & Francis Group

RESEARCH PAPER

Non-muscle MYH10/myosin IIB recruits ESCRT-III to participate in autophagosome closure to maintain neuronal homeostasis

Yong-Woo Jun[a], Soojin Lee[a], Byung-Kwan Ban[b], Jin-A Lee[b], and Fen-Biao Gao[a]

[a]Department of Neurology, University of Massachusetts Chan Medical School, Worcester, MA, USA; [b]Department of Biotechnology and Biological Sciences, Hannam University, Yuseong-gu, Daejeon, Republic of Korea

ABSTRACT

Dysfunction of the endosomal sorting complex required for transport (ESCRT) has been linked to frontotemporal dementia (FTD) due in part to the accumulation of unsealed autophagosomes. However, the mechanisms of ESCRT-mediated membrane closure events on phagophores remain largely unknown. In this study, we found that partial knockdown of non-muscle MYH10/myosin IIB/zip rescues neurodegeneration in both *Drosophila* and human iPSC-derived cortical neurons expressing FTD-associated mutant CHMP2B, a subunit of ESCRT-III. We also found that MYH10 binds and recruits several autophagy receptor proteins during autophagosome formation induced by mutant CHMP2B or nutrient starvation. Moreover, MYH10 interacted with ESCRT-III to regulate phagophore closure by recruiting ESCRT-III to damaged mitochondria during PRKN/parkin-mediated mitophagy. Evidently, MYH10 is involved in the initiation of induced but not basal autophagy and also links ESCRT-III to mitophagosome sealing, revealing novel roles of MYH10 in the autophagy pathway and in ESCRT-related FTD pathogenesis.

Abbreviations: ALS: amyotrophic lateral sclerosis; AP: autophagosome; Atg: autophagy-related; ESCRT: endosomal sorting complex required for transport; FTD: frontotemporal dementia

ARTICLE HISTORY
Received 30 September 2022
Revised 11 January 2023
Accepted 12 January 2023

KEYWORDS
Autophagy; *Drosophila*; ESCRT; mitophagy; myosin II; neurodegeneration; neuron

Introduction

The accumulation of misfolded proteins in neurons is a pathological hallmark of many neurodegenerative diseases. Protein homeostasis is critically important for neuronal health and function. A major proteostasis pathway that has been intensely investigated in recent decades is autophagy (referring to macroautophagy herein), an intracellular process to engulf cytoplasmic contents such as proteins, RNAs, and damaged organelles into double-membrane autophagosomes that fuse with lysosomes for eventual degradation [1]. The molecular machineries of several steps in autophagosome formation are fairly well understood. For instance, a set of ATG proteins forms different multimeric protein complexes with ULKs and RB1CC1/FIP200 or with BECN1/beclin 1 and PIK3C3/VSP34 and other proteins in a sequential manner to regulate the induction or nucleation of phagophores [1,2]. This early step is regulated by the MTOR (mammalian target of rapamycin) pathway and thus can be activated by nutrition starvation or rapamycin [3,4]. Other regulators of autophagy include some myosin families of motor proteins. For example, in *Drosophila*, Atg1 activates sqh/myosin II which in turn regulates starvation-induced autophagy [5]. In mammalian cells, both MYO6/myosin VI [6] and MYO1C/myosin 1C [7] regulate autophagosome maturation and its fusion with the lysosome. The regulatory function of other myosin proteins in different autophagy steps remains unknown, especially in mammalian neurons.

Autophagy is especially important for the survival and function of long-lived postmitotic neurons: any defect along this clearance pathway may contribute to disease pathogenesis through various mechanisms of neurodegeneration [8,9]. For instance, partial loss of C9orf72 activity contributes to amyotrophic lateral sclerosis (ALS) and frontotemporal dementia (FTD), in part through the ULK1-induced decrease in autophagy [10–13]. In this case, pharmacological treatments to enhance autophagy induction (e.g., by rapamycin) alleviate ALS-FTD disease phenotypes in cellular models [14,15]. Conversely, excess accumulation of abnormal autophagosomes contributes to neurodegeneration, for instance, through defects in autophagosome maturation caused by FTD-associated mutant CHMP2B, a subunit of endosomal sorting complex required for transport–III (ESCRT-III) [16,17].

The molecular mechanisms of autophagosome maturation and its role in neurodegeneration are less understood than those of autophagy induction; in particular, it is largely unknown how autophagosome membranes are sealed before fusion with lysosomes. Since ESCRTs are required for autophagosome maturation [17–19] and have well-established roles in membrane budding and scission, it has long been speculated that the ESCRT machinery may be directly involved in autophagosome closure [20]. Indeed, knockdown of the ESCRT-III subunit CHMP4B leads to the accumulation of multilamellar structures that are LC3-II- and STX12/STX13

CONTACT Fen-Biao Gao fen-biao.gao@umassmed.edu Department of Neurology, University of Massachusetts Chan Medical School, Worcester, MA 01605, USA

Supplemental data for this article can be accessed online at https://doi.org/10.1080/15548627.2023.2169309

(syntaxin 12)-positive abnormal autophagosomes [17,21]. Thus, without ESCRT-III activity, autophagosome membranes may fail to seal and therefore continue to grow into multilamellar structures. More recent studies have revealed a direct role for ESCRT-III in autophagosome closure [22–26]. However, it is not known how, or which, proteins help recruit ESCRTs to unsealed autophagosome membranes to perform this critical function.

In this study, we show that partial knockdown of non-muscle MYH10 rescues neurodegeneration caused by FTD-associated mutant CHMP2B. We also reveal a novel role for MYH10 in recruiting ESCRT-III to autophagosome membrane sealing, providing new insights into the autophagy pathway and ESCRT-related FTD pathogenesis.

Results

MYH10 is a novel genetic suppressor of FTD-associated mutant CHMP2B toxicity

Previously, we identified several genetic modifiers whose partial loss of function enhanced the toxicity of FTD-associated mutant CHMP2B in *Drosophila* [27–29]. To facilitate the investigation of potential genetic suppressors, we raised flies expressing mutant CHMP2B (CHMP2B^{intron5}) in the eye under the control of *GMR-Gal4* at 27°C instead of 25°C so that all the flies showed a severe retinal degeneration phenotype (Figure 1A, B). Two different RNAi lines that knock down *zip* (zipper) by 25–55% (Figure 1C) suppressed retinal degeneration caused by mutant CHMP2B (Figure 1A, B), indicating that the toxicity of mutant CHMP2B is highly sensitive to *zip* dosage. Mutant CHMP2B toxicity was also greatly reduced in flies expressing a genetic allele of *zip* (*zip*^{1}) that results in a loss of function in the gene (Figure 1D) [30] (Figure 1A, B). Thus, *zip* is a strong novel genetic suppressor of FTD-associated mutant CHMP2B toxicity in *Drosophila*.

Zip encodes the MYH10 homolog, the non-muscle motor protein that transports cargos on actin filaments [30,31]. In human neurons, MYH10/myosin IIB is expressed at a substantially higher level than MYH9/myosin IIA and MYH11/myosin IIC [32]. To test whether MYH10 genetically modifies mutant CHMP2B toxicity in mammalian neurons,

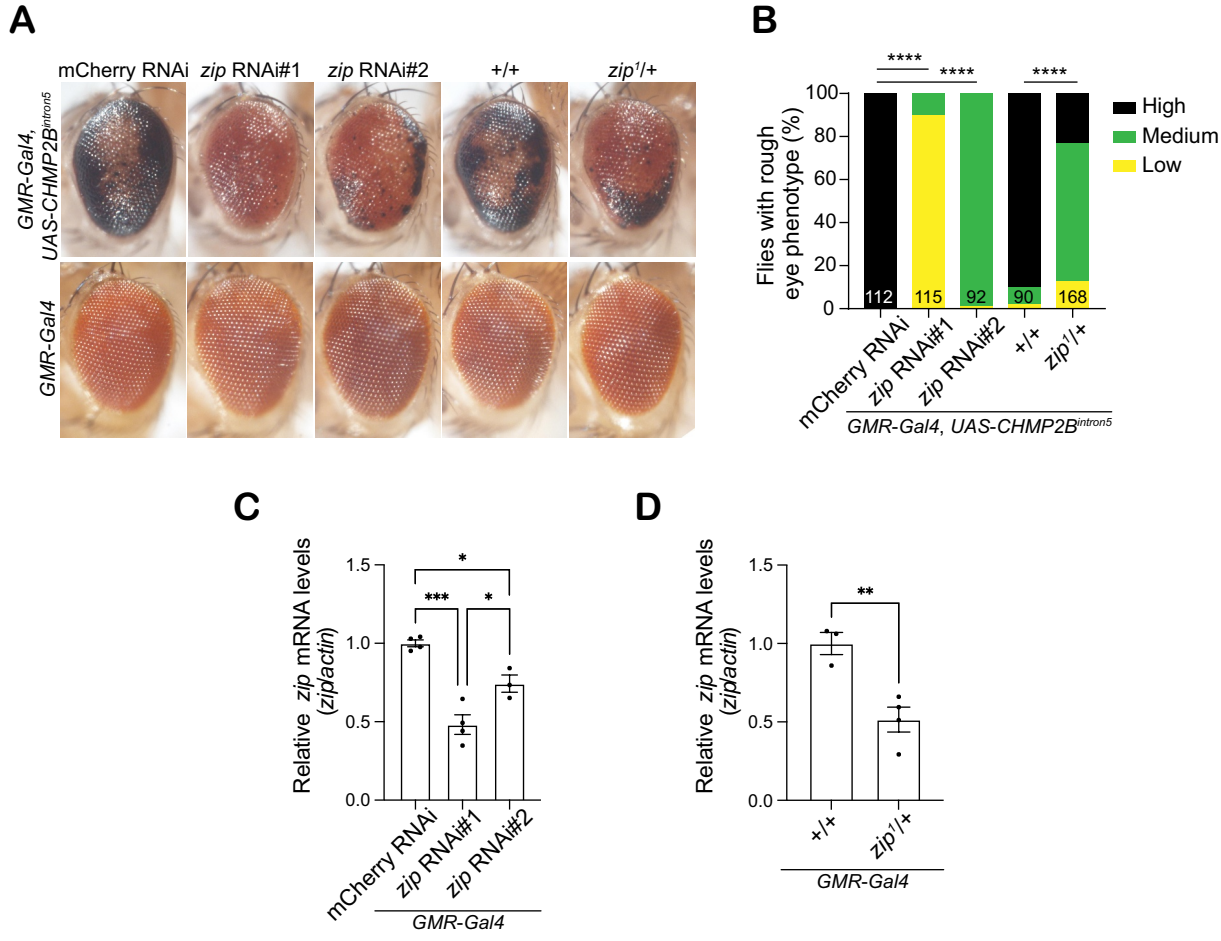

Figure 1. Partial inhibition of *zip* rescues neurodegeneration caused by FTD-associated mutant CHMP2B (CHMP2B ^{intron5}) in *Drosophila*. (A) Representative images of retinal degeneration in adult flies of different genotypes. Eyes of control flies expressing mCherry RNAi alone had normal ommatidial organization. CHMP2B^{intron5} expression led to rough eye and loss-of-pigmentation phenotypes. The morphological defects were partially rescued by two independent *zip* RNAi lines or by the *zip*^{1} heterozygous mutant allele. (B) Quantification of genetic interactions between CHMP2B^{intron5} and *zip* in the *Drosophila* eye. The total number of flies of each genotype is shown in each column. ****$P < 0.0001$ by chi-square test. (C-D) Silencing of *Zip* in *Drosophila* by RNAi or heterozygous mutant *zip* allele. Real-time quantitative PCR analysis of *zip* mRNA expression levels in two independent RNAi lines (C) and *zip*^{1} heterozygous mutant allele (D) compared to control flies. *$P <$ 0.05, **$P < 0.01$, ***$P < 0.001$, ****$P < 0.0001$ by one-way ANOVA with Tukey post-hoc test for multiple comparisons or paired two-tailed *t* test.

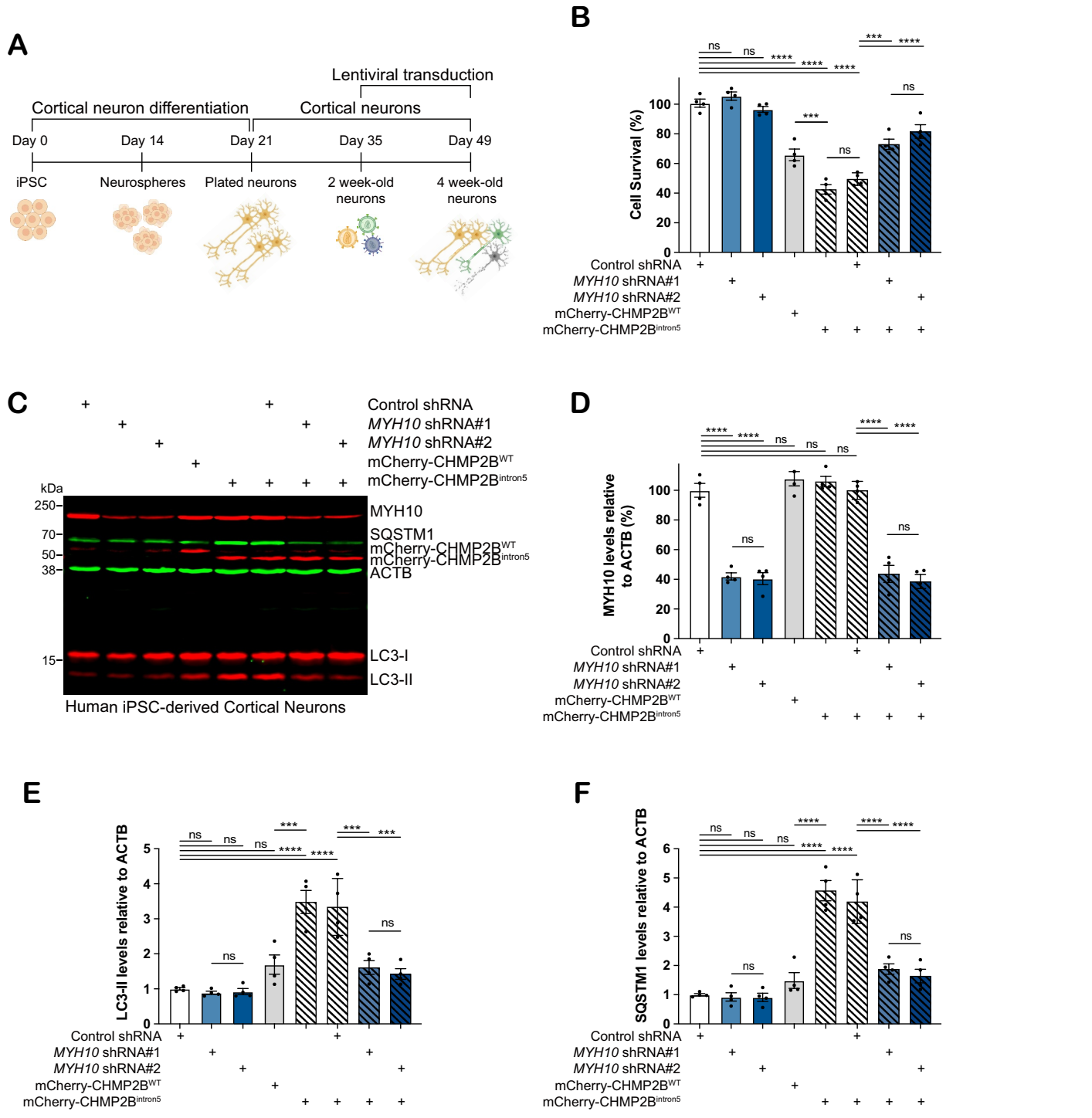

Figure 2. Knockdown of *MYH10* suppresses neurodegeneration caused by FTD-associated mutant CHMP2B in iPSC-derived cortical neurons. (A) Schematic of the experimental timeline of the differentiation of cortical neurons from iPSCs and the lentiviral transduction strategy. (B) Viability of iPSC-derived cortical neurons transfected with CHMP2B^{WT}, CHMP2B^{intron5}, and control or *MYH10* shRNAs. Values are mean ± SEM of 4 biologically independent experiments. *$P < 0.05$, **$P < 0.01$, ***$P < 0.001$, ****$P < 0.0001$ by one-way ANOVA with Tukey post-hoc test for multiple comparisons. (C) Western blot analysis of the lysates of iPSC-derived cortical neurons with anti-MYH10, anti-SQSTM1, anti-CHMP2B, anti-ACTB/β-actin, or anti-LC3 antibodies. (D-F) Quantification of *MYH10* knockdown (D) and autophagic flux based on the ratio of LC3-II (E) or SQSTM1 (F) relative to ACTB in iPSC-derived cortical neurons. Values are mean ± SEM of 4 biologically independent experiments. *$P < 0.05$, **$P < 0.01$, ***$P < 0.001$, ****$P < 0.0001$, ns, not significant, by one-way ANOVA with Tukey post-hoc test for multiple comparisons.

we differentiated human induced pluripotent stem cells (iPSCs) into cortical neurons (Figure 2A) as previously described [33]. Expression of mutant CHMP2B caused about half of the human iPSC-derived neurons to die (Figure 2B), while knocking down *MYH10* with two different shRNAs partially suppressed neuronal cell death induced by mutant CHMP2B (Figure 2B). The *MYH10* knockdown efficiency by these shRNAs is about 60% as shown by western blot analysis

(Figure 2C, D). Thus, MYH10 mediates mutant CHMP2B-induced neurodegeneration in human iPSC-derived neurons as well.

MYH10 is required for the activation of mutant CHMP2B-, starvation-, or CCCP-induced autophagy but not basal autophagy

Previously, we found that expression of mutant CHMP2B protein or knockdown of the *CHMP4B* gene blocks autophagosome maturation, resulting in the accumulation of multilamellar structures [17,21]. Moreover, knocking down *ATG5*, a key protein in autophagy induction [34], partially rescues neuronal cell death induced by mutant CHMP2B [16], indicating a detrimental effect of the accumulation of abnormal autophagosomes in neurons. To determine whether MYH10 also participates in the autophagy pathway and if so, whether this function underlies its modulation of mutant CHMP2B toxicity, we performed western blot analysis to investigate the molecular consequences of *MYH10* knockdown by two different shRNAs in iPSC-derived human cortical neurons. We found that *MYH10* knockdown did not affect the ratio between actin and LC3-II (Figure 2C, E), a standard marker for autophagosomes, or the level of SQSTM1/p62 (Figure 2C, F), an autophagic substrate and receptor protein, under normal conditions, suggesting that MYH10 does not play a role in basal autophagy. Consistent with previous reports [16,17], expression of mutant CHMP2B increased the LC3-II: actin ratio (Figure 2C, E), as well as the SQSTM1 level (Figure 2C, F). These increases were greatly attenuated by *MYH10* knockdown (Figure 2C, E, and F), indicating that MYH10 is involved in mutant CHMP2B-induced accumulation of autophagosomes.

To further examine the role of MYH10 in regulating autophagy, we used CRISPR-Cas9 technology to delete *MYH10* in U2OS cells, and confirmed the deletion via immunoblotting analysis (Figure S1A-C). *MYH10* knockout (KO) cells were viable, and basal autophagy in these cells was unaffected, as the levels of LC3-II and SQSTM1 remained the same as in wild-type cells (Figure 3A-C), again indicating that MYH10 is not required for basal autophagy. As expected, amino acid starvation greatly increased the level of LC3-II in wild-type cells; however, the increase was greatly attenuated in *MYH10* KO cells, and statistical analysis indicates that *MYH10* KO cells completely failed to initiate starvation-induced autophagy (Figure 3A, B). Moreover, starvation-induced autophagy decreased the level of SQSTM1 in wild-type, but not in *MYH10* KO cells (Figure 3A, C), suggesting that MYH10 is responsible for maintaining autophagic flux. Loss of MYH10 attenuated the increase in the LC3-II level and the decrease in the SQSTM1 level induced by starvation and bafilomycin A_1 treatment (BafA1, a specific inhibitor of the vacuolar-type H^+-ATPase) (Figure 3A-C). Consistent with the western blot analysis mentioned above, *MYH10* KO cells showed a significantly attenuated increase in the number of LC3-II and SQSTM1-positive autophagosomes compared with wild-type cells in the presence of starvation or starvation and BafA1 (Figure 3D-F). Together, these findings indicate that MYH10 is not required for basal autophagy but is involved in autophagy induction caused by amino acid starvation, and degradation.

We predict a potential role of MYH10 in mitophagy, as defects in this process are common in many neurodegenerative diseases [35–37]. Carbonyl cyanide m-chlorophenyl hydrazone (CCCP) compromised mitochondria function and thus activated mitophagy, as shown by recruitment of PRKN/parkin and LC3 to damaged mitochondria (Figure 4A). Interestingly, MYH10 colocalized with PRKN- and LC3-positive puncta containing mitochondria (Figure 4B, C). More importantly, the number of LC3-positive mitophagosomes, relative to PRKN-positive damaged mitochondria, and the relative percentage of mitophagosomes were decreased in *MYH10* KO cells. This indicates a functional role for MYH10 in mitophagosome formation (Figure 4D-F).

MYH10 recruits autophagy receptor proteins to newly formed phagophores

To investigate the exact role of MYH10 in induced autophagy, we evaluated the interaction between MYH10 and autophagic receptor proteins that: bind to LC3 on the phagophore membrane, are incorporated into autophagosomes, and function as receptors for ubiquitinated cargos [38–40]. During autophagy, these receptor proteins recognize and recruit damaged cargos to phagophores by interacting with cytoskeletal proteins [41]. Intriguingly, we found that MYH10 binds to several autophagic receptor proteins under either basal conditions or starvation conditions, including SQSTM1, OPTN (optineurin), and CALCOCO2/NDP52, in co-immunoprecipitation experiments (Figure 5A). This biochemical interaction was confirmed by confocal fluorescence imaging, which showed that MYH10 partially colocalizes with these receptor proteins in transfected cells (Figure 5B).

We also performed immunofluorescence experiments to determine whether MYH10 affects the recruitment of autophagic receptor proteins to damaged mitochondria. Interestingly, the recruitment of SQSTM1 (Figure 5C-E) or OPTN (Figure 5F-H) to PRKN-positive damaged mitochondria is decreased in *MYH10* KO cells, suggesting that MYH10 helps transport autophagy receptor proteins to degradation cargos during mitophagy induction.

MYH10 interacts with and recruits ESCRT-III components to damaged mitochondria during mitophagosome sealing

To further understand the role of MYH10 in the autophagy pathway, we expressed tagged MYH10 and several components of the ESCRT-III complex in HEK293T cells. Co-immunoprecipitation experiments showed that MYH10 physically interacts with CHMP2B, CHMP4A, CHMP4B, and CHMP4C (Figure 6A). Confocal fluorescent imaging showed that MYH10 partially colocalizes with wild-type or mutant CHMP2B, as well as CHMP4A, CHMP4B, or CHMP4C (Figure 6B). In contrast to diffusely localized CHMP2B, CHMP4 family proteins are known to form oligomers. Thus, ectopically-expressed CHMP4A, CHMP4B, or CHMP4C appear to strongly colocalize with MYH10 in aggregates (Figure 6B). CHMP4B is the most abundant family member in mammalian neurons [42] and is highly recruited to autophagosomes [43], and thus we further

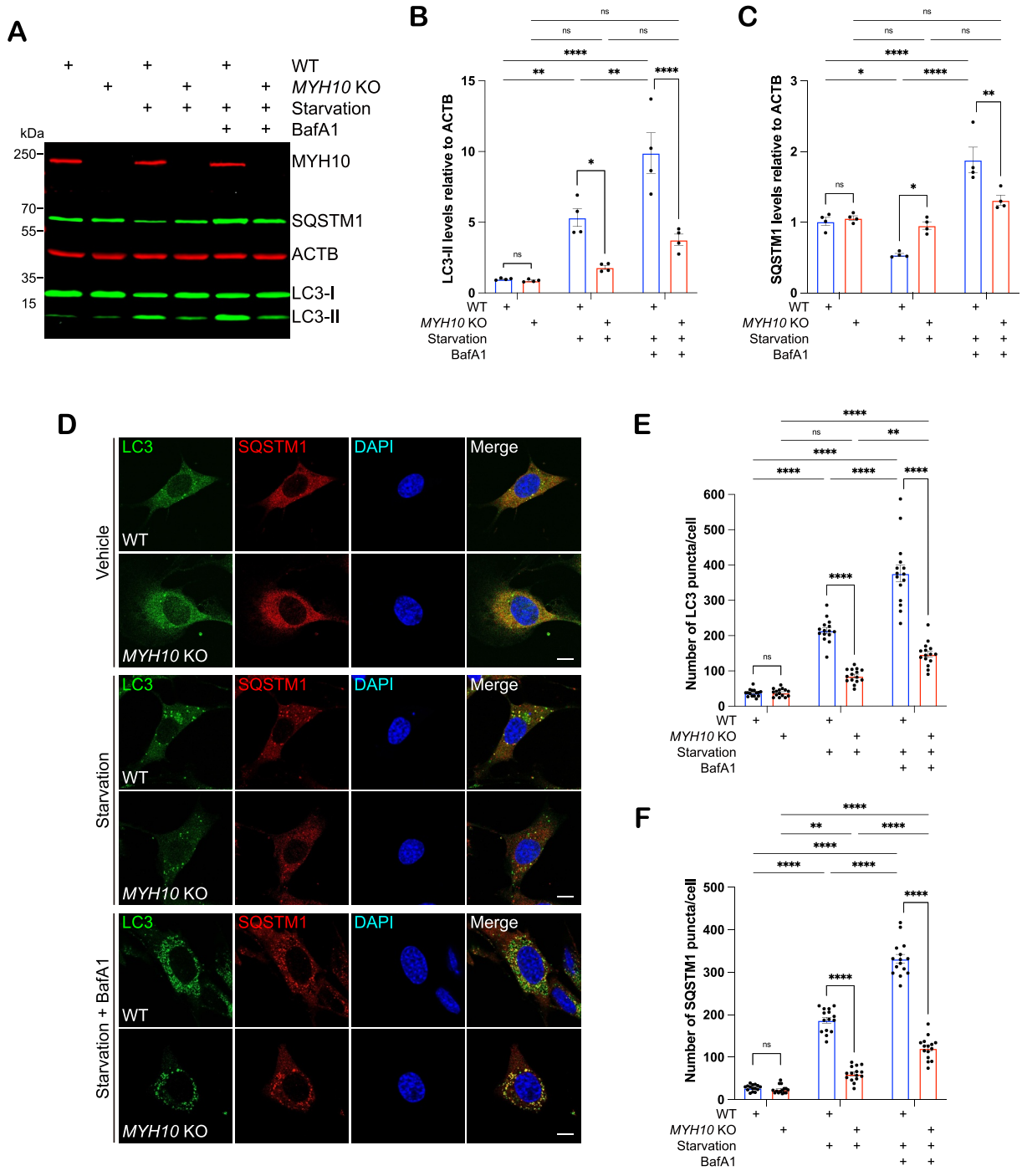

Figure 3. MYH10 is essential for autophagosome formation. (A) Autophagic flux assay. Lysates of wild-type (WT) or *MYH10* knockout (KO) U2OS cells were subjected to amino acid starvation in the absence or presence of bafilomycin A_1 (BafA1, 100 nM) for 2 h and analyzed by western blot with antibodies against MYH10, SQSTM1, ACTB, or LC3. (B-C) Quantification of autophagic flux based on the difference of LC3-II (B) or SQSTM1 (C) relative to ACTB in WT or *MYH10* KO U2OS cells. Values are mean ± SEM of 4 biologically independent experiments. $^{*}P < 0.05$, $^{**}P < 0.01$, $^{***}P < 0.001$, $^{****}P < 0.0001$ by two-way ANOVA followed by Tukey's post hoc test for multiple comparisons. (D) Representative immunofluorescence images of LC3- and SQSTM1-positive autophagosomes in wild-type (WT) or *MYH10* knockout (KO) U2OS cells after amino acid starvation in the absence or presence of bafilomycin A_1 (BafA1, 100 nM) for 2 h. Scale bar: 20 µm. (E-F) Number of LC3- (E) or SQSTM1-positive (F) puncta per cell. Cells were counted with the ITCN plugin using FIJI. Values are mean ± SEM of $n > 15$ randomly selected cells. $^{****}P < 0.0001$, ns, not significant by two-way ANOVA followed by Tukey's post hoc test for multiple comparisons.

studied this protein. In reverse immunoprecipitation experiments in HEK293T cells, endogenous CHMP4B also selectively interacted with endogenous MYH10 but not with MYO5B/myosin VB (Figure 6C). CHMP4B contains several alpha helical structures that undergo conformational rearrangement upon binding to the membrane [44–48] (Figure 6D). We found that both the N-terminal and C-terminal halves of CHMP4B are involved in binding to MYH10 (Figure 6E). In addition, deletion analysis (Figure 6F) showed that the C-terminal end of MYH10 binds to CHMP4B (Figure 6G, H) or CHMP2B (Figure S2).

Previously we reported that *CHMP4B* knockdown resulted in the accumulation of multilamellar structures that resemble

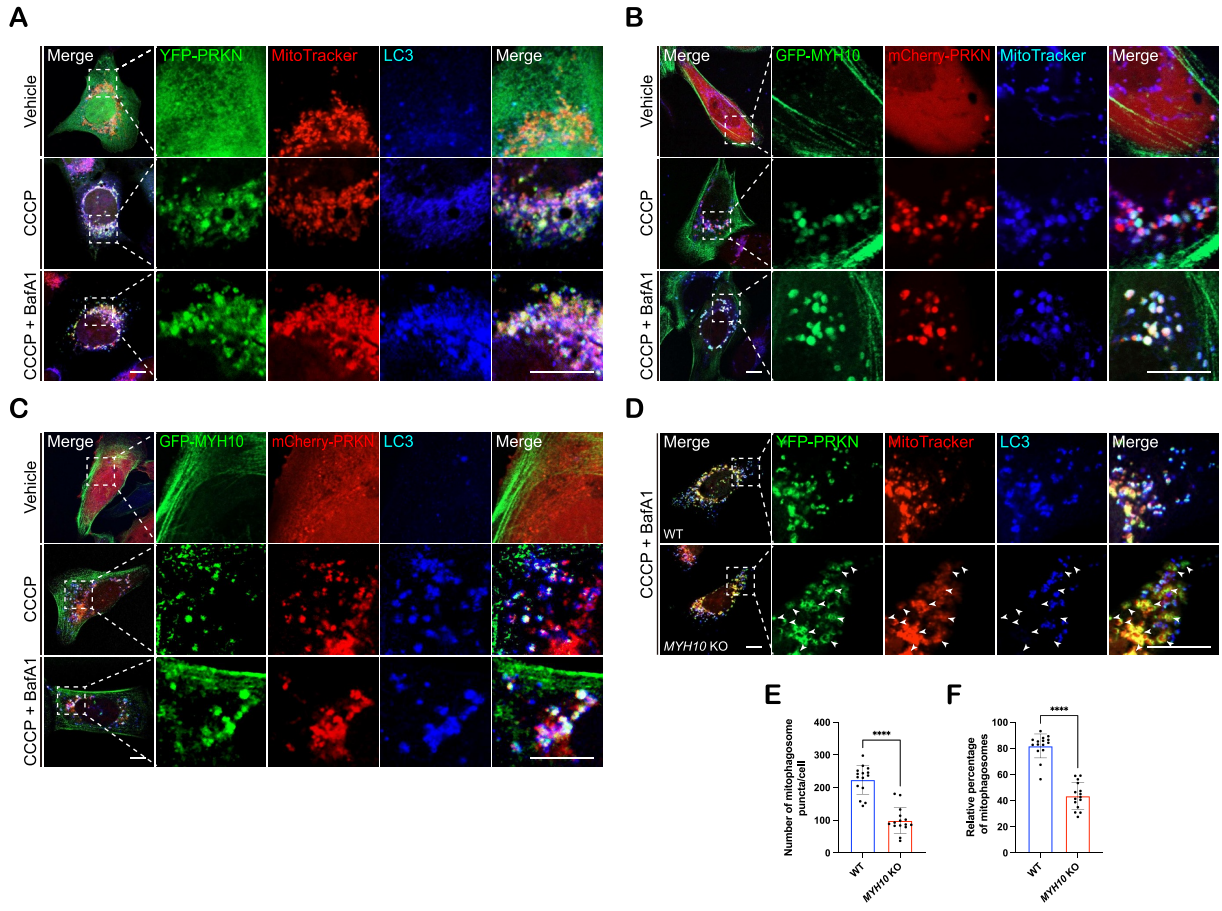

Figure 4. MYH10 is involved in PRKN-mediated mitophagy. (A-C) Representative immunofluorescence images showing PRKN-mediated mitophagy. U2OS cells stably expressing YFP-PRKN were stained with MitoTracker (red) and antibodies against LC3 (A). U2OS cells stably expressing GFP-MYH10 and mCherry-PRKN were stained with MitoTracker (blue) (B) or antibodies against LC3 (C). The cells were treated for 2 h with carbonyl cyanide m-chlorophenyl hydrazone (CCCP, 20 μM) or with CCCP and bafilomycin A_1 (BafA1, 100 nM). Scale bar: 20 μm. (D) Cells stably expressing YFP-PRKN were stained with MitoTracker (red) and antibodies against LC3. The cells were treated with carbonyl cyanide m-chlorophenyl hydrazone (CCCP, 20 μM) and bafilomycin A_1 (BafA1, 100 nM) for 2 h. White arrowheads indicate PRKN-dependent and LC3-independent mitochondria. Scale bar: 20 μm. (E-F) Number and relative percentage of PRKN- and LC3-positive mitophagosomes, which was calculated as the number of LC3-positive mitophagosomes divided by the total number of PRKN-positive damaged mitochondria. Values are mean ± SEM of $n > 15$ randomly selected cells. $^{****}P < 0.0001$ by paired two-tailed t test.

autophagosomes, raising the possibility that ESCRT-III is involved in autophagosome sealing [21]. Indeed, recent studies have revealed a direct role for ESCRT-III in autophagic membrane sealing events [22–26]. Since MYH10 interacts with ESCRT-III, we examined whether MYH10 is also involved in autophagosome closure. We found that down-regulation of *CHMP4B* with siRNA increased the expression of LC3-II and SQSTM1 in all three conditions, including basal, starvation-, or CCCP-induced autophagy in wild-type cells (Figure S3), further supporting the notion CHMP4B plays a key role in autophagy. Furthermore, starvation or CCCP treatment increased the LC3-II level and decreased the SQSTM1 level in wild-type cells, but not in *MYH10* KO cells as determined by statistical analysis of the results (Figure S3), suggesting that MYH10 affects both starvation- or CCCP-induced autophagy and degradation. These results demonstrate overlapping but distinct functions of MYH10 and CHMP4B in basal and stress-induced autophagy. Interestingly, both the number and the percentage of STX17/syntaxin 17-positive mature autophagosomes were reduced in *MYH10* KO cells, a phenotype identical to that seen after siRNA-mediated knockdown of *CHMP4B* (Figure 7A-C). In addition, the percentage of STX17-positive mature autophagosomes after *CHMP4B* knockdown in *MYH10* KO cells is not significantly different from that of *CHMP4B* knockdown or *MYH10* KO cells, supporting the notion that MYH10 and ESCRT-III are involved in autophagosome maturation and act together for autophagic degradation (Figure 7A-C).

In addition to starvation-induced autophagy (Figure 7A-C), the relative percentage of STX17-positive mature mitophagosomes was significantly decreased in *MYH10* KO cells upon mitophagy induction by CCCP treatment (Figure 7D-F), suggesting MYH10 could be involved in mitophagosome maturation. Importantly, the recruitment of CHMP4B to CCCP-induced damaged mitochondria was greatly compromised in *MYH10* KO cells (Figure 8A-C). Together with our findings that MYH10 physically interacts with CHMP4B and other ESCRT-III subunits (Figure 6 and Figure S2), these results indicate a direct role for MYH10 in recruiting ESCRT-III to mitophagosomes. Since ESCRT-III is involved in phagophore closure [21–23,25,26,43], we reasoned that MYH10

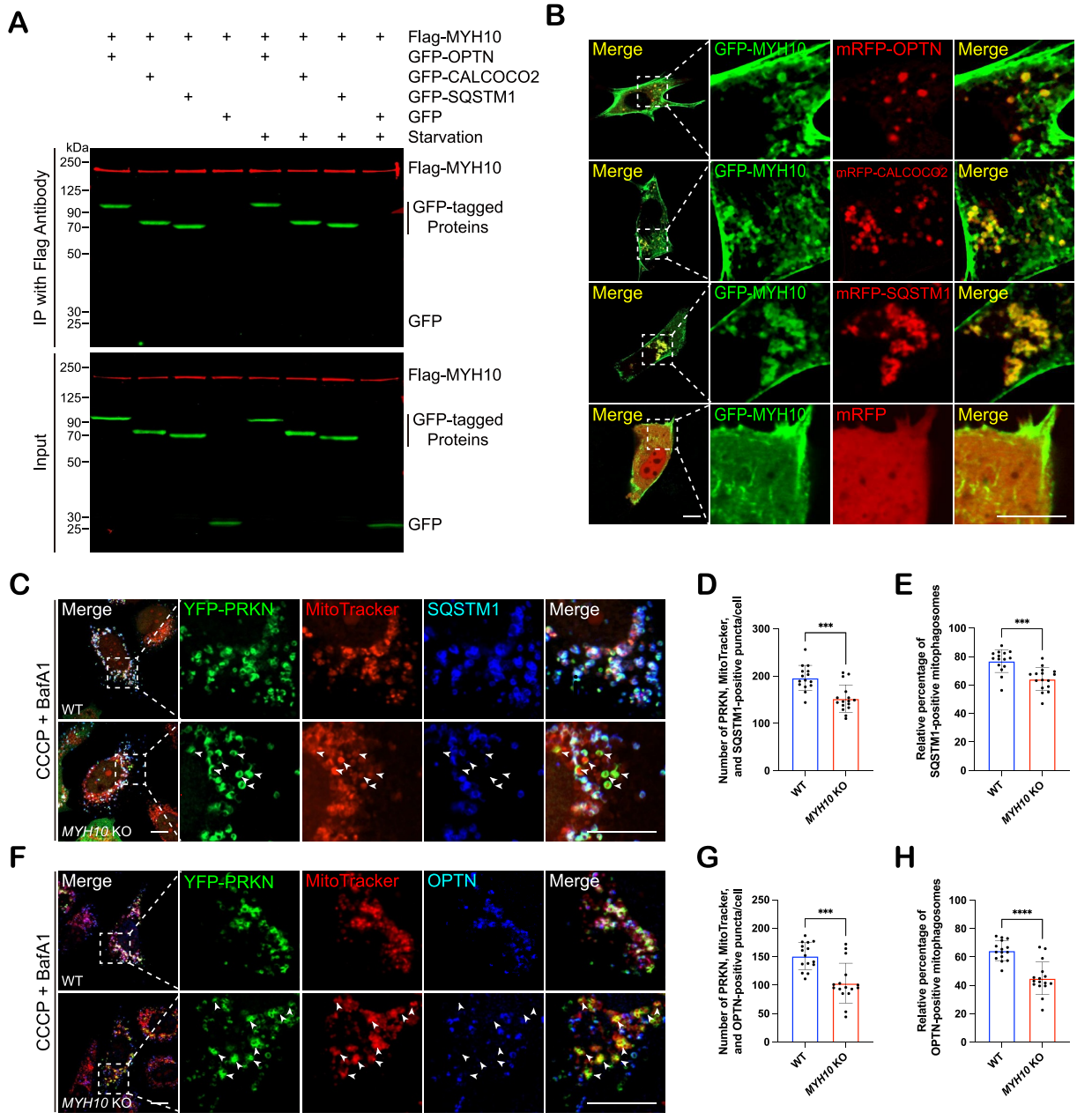

Figure 5. MYH10 recruits autophagic receptor proteins to autophagosomes. (A) Co-immunoprecipitation analysis of MYH10 and autophagic receptors. HEK293T cells were transfected with vectors expressing proteins tagged with Flag-MYH10 and green fluorescent proteins (GFP, GFP-OPTN, GFP-CALCOCO2, or GFP-SQSTM1), and were subjected to co-immunoprecipitation with anti-Flag agarose beads in the absence or presence of amino acid starvation for 2 h. Western blotting was done with anti-Flag antibody or anti-GFP antibody. (B) Cellular localization of GFP-MYH10 with monomeric red fluorescent protein (mRFP)-autophagic receptors (OPTN, CALCOCO2, and SQSTM1). U2OS cells stably expressing GFP-MYH10 were transiently transfected with mRFP-OPTN, -CALCOCO2, or -SQSTM1. Scale bar: 20 μm. (C and F) Cells stably expressing YFP-PRKN were stained with MitoTracker (red) and antibodies against SQSTM1 (C) or OPTN (F) and treated with carbonyl cyanide m-chlorophenyl hydrazone (CCCP, 20 μM) and bafilomycin A_1 (BafA1, 100 nM) for 2 h. White arrowheads indicate PRKN-positive and SQSTM1- (C) or OPTN-negative (F) mitochondria. Scale bar: 20 μm. (D-H) Number and relative percentage of PRKN- and SQSTM1- (D and E) or OPTN-positive (G and H) mitophagosomes, which was calculated as the number of SQSTM1- or OPTN-positive mitophagosomes divided by the total number of PRKN-positive damaged mitochondria. Values are mean ± SEM of $n > 15$ randomly selected cells. $^{*}P < 0.05$, $^{**}P < 0.01$, $^{***}P < 0.001$, $^{****}P < 0.0001$ by paired two-tailed t test.

should play a direct role in this cellular process as well. Indeed, multilamellar structures containing damaged mitochondria accumulated in *MYH10* KO cells (Figure 8D), a phenotype identical to that caused by *CHMP4B* knockdown (Figure 8D). The efficiency and consequences of *CHMP4B* knockdown in wild-type and *MYH10* KO cells were assessed by western blot (Figure S3D). Thus, we propose that MYH10 recruits ESCRT-III to unsealed autophagosomes to facilitate closure, providing a novel molecular insight into mechanisms of ESCRT-III assembly on autophagosome membranes (Figure S4).

Discussion

This study shows that partial knockdown of non-muscle MYH10 rescues neurodegeneration caused by FTD-

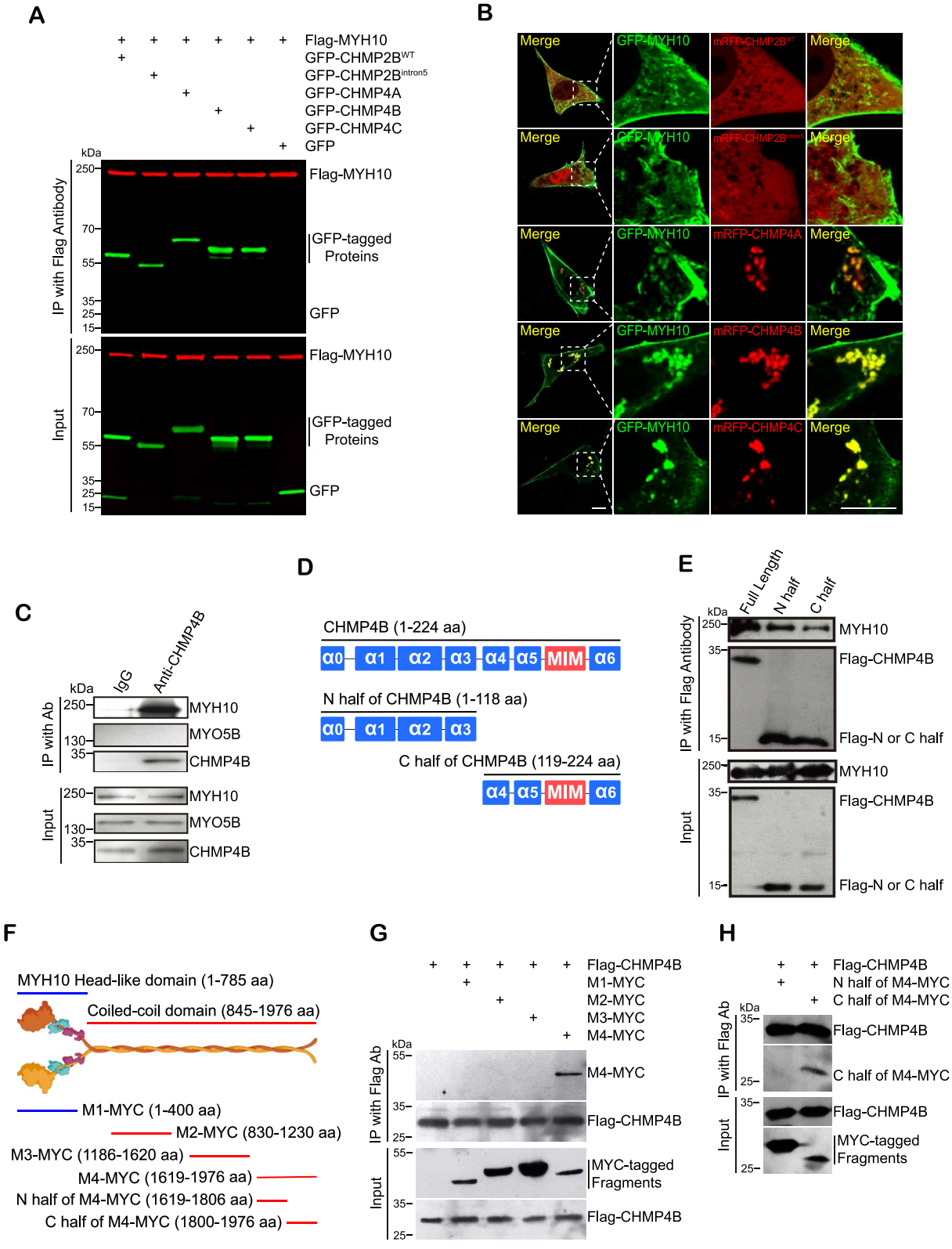

Figure 6. A novel biochemical interaction between MYH10 and ESCRT-III. (A) Co-immunoprecipitation analysis of MYH10 and ESCRT-III subunits (CHMP2B^{WT}, CHMP2B^{intron5}, CHMP4A, CHMP4B, and CHMP4C). HEK293 cells were transfected with vectors expressing proteins tagged with Flag-MYH10 and green fluorescent proteins (GFP, GFP-CHMP2B^{WT}, -CHMP2B^{intron5}, -CHMP4A, -CHMP4B, or -CHMP4C) Co-immunoprecipitation with anti-Flag agarose beads and western blotting were done with anti-Flag antibody or anti-GFP antibody. (B) Cellular localization of MYH10 with ESCRT-III subunits. U2OS cells stably expressing GFP-MYH10 were transiently transfected with mRFP-CHMP2B^{WT}, -CHMP2B^{intron5}, -CHMP4A, -CHMP4B, or -CHMP4C. Scale bar: 20 μm. (C) Interaction of endogenous proteins CHMP4B and MYH10. HEK293T cell lysates were immunoprecipitated with anti-CHMP4B antibody; nonimmune IgG served as negative control. Western blotting was done with antibodies against MYH10, MYO5B, or CHMP4B. (D) Schematic diagram of the domain structure of CHMP4B. CHMP4B contains six α-helices and a microtubule-interacting and transport (MIT)-interacting motif (MIM) that mediates VPS4 binding. (E) Immunoprecipitation analysis of the interaction between endogenous MYH10 and full-length (FL) or various deletion mutants of CHMP4B. Flag-tagged proteins (Flag-CHMP4B full length, N-terminal half of CHMP4B (residues 1–118), or C-terminal half of CHMP4B (residues 119–224) were transfected in HEK293T cells, and immunoprecipitation was done with anti-Flag agarose beads. Western blotting was done with anti-Flag antibody or anti-MYH10 antibody. (F) Schematic diagram of the domain structure of MYH10. MYH10 has a head-like domain and coiled-coil domain. (G-H) Immunoprecipitation analysis of the interaction between CHMP4B and various deletion mutants of MYH10. Flag-CHMP4B and MYC/cMyc-tagged proteins (M1-, M2-, M3-, M4-, N-terminal half of M4-, or C-terminal half of M4-MYC) were transfected into HEK293T cells and co-immunoprecipitated with anti-Flag agarose beads. Western blotting was done with anti-Flag antibody or anti-MYC antibody.

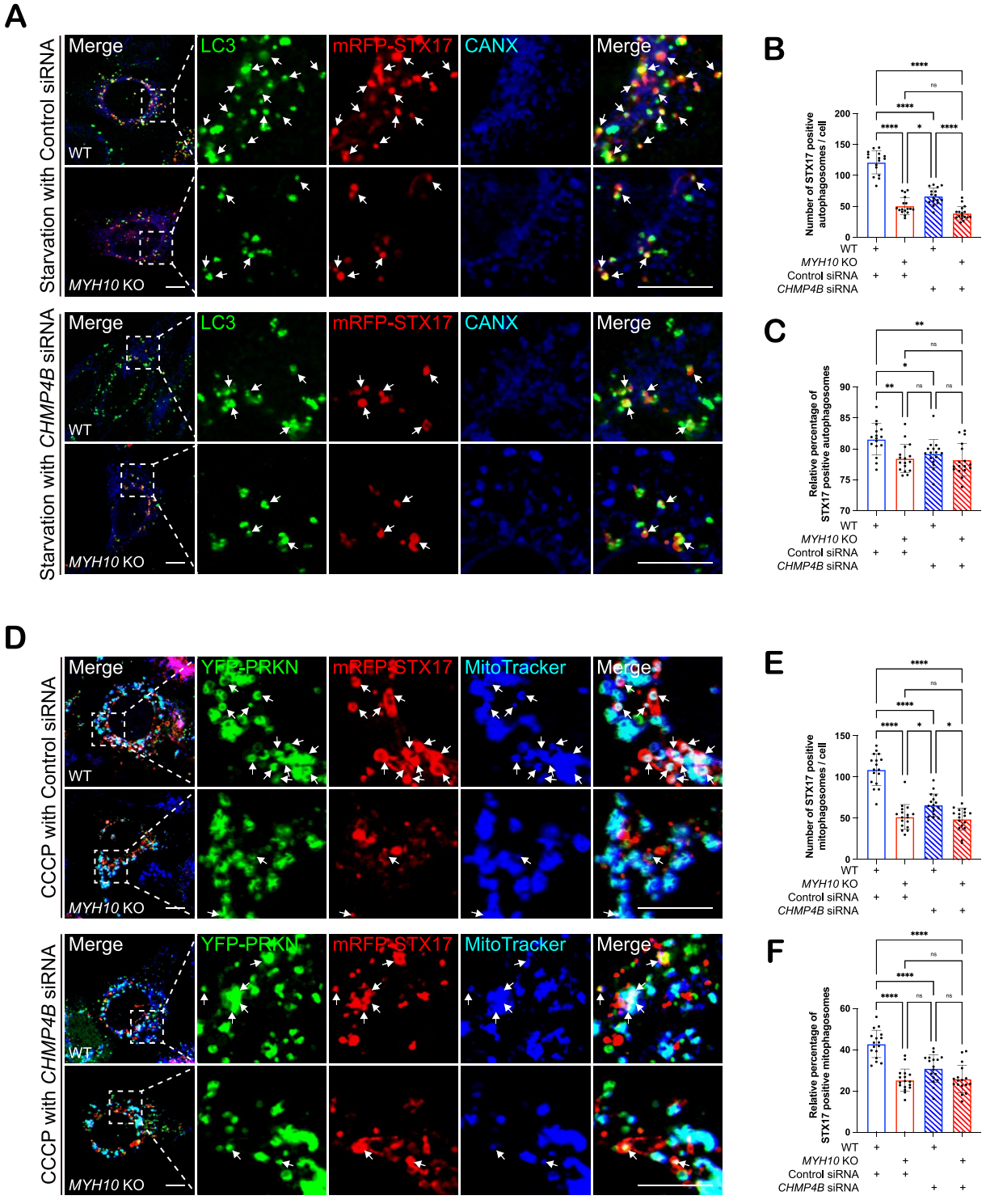

Figure 7. MYH10 is involved in phagophore closure. (A) Representative immunofluorescence images showing completed autophagosomes (completely sealed autophagosomes) in WT or *MYH10* KO U2OS cells stably expressing mRFP-STX17. The cells were stained with antibodies against LC3 and CANX (calnexin), an endoplasmic reticulum (ER) marker, and were subjected to amino acid starvation in the absence or presence of *CHMP4B* knockdown. White arrows indicate LC3- and STX17-positive completely closed autophagosomes. Scale bar: 20 μm. (B-C) Number and relative percentage of STX17-positive completed autophagosomes, which was calculated as the number of STX17-positive autophagosomes divided by the total number of LC3-positive autophagosomes. The cells were counted with the ITCN plugin using FIJI. Values are mean ± SEM of >16 randomly selected cells. $^{*}P < 0.05$, $^{**}P < 0.01$, $^{***}P < 0.001$, $^{****}P < 0.0001$ by one-way ANOVA with Tukey's post hoc test for multiple comparisons. (D) U2OS cells stably expressing YFP-PRKN and mRFP-STX17 were stained with MitoTracker (blue) after treated with carbonyl cyanide m-chlorophenyl hydrazone (CCCP, 20 μM) for 2 h in the absence or presence of *CHMP4B* knockdown. White arrows indicate PRKN- and STX17-positive completely closed mitophagosomes. Scale bar: 20 μm. (E-F) Number and relative percentage of PRKN- and STX17-positive mitophagosomes. which was calculated as the number of STX17-positive mitophagosomes divided by the total number of PRKN-positive damaged mitochondria. WT, wild-type; KO, knockout. Values are mean ± SEM of $n > 17$ randomly selected cells. $^{*}P < 0.05$, $^{**}P < 0.01$, $^{***}P < 0.001$, $^{****}P < 0.0001$ by one-way ANOVA with Tukey's post-hoc test for multiple comparisons.

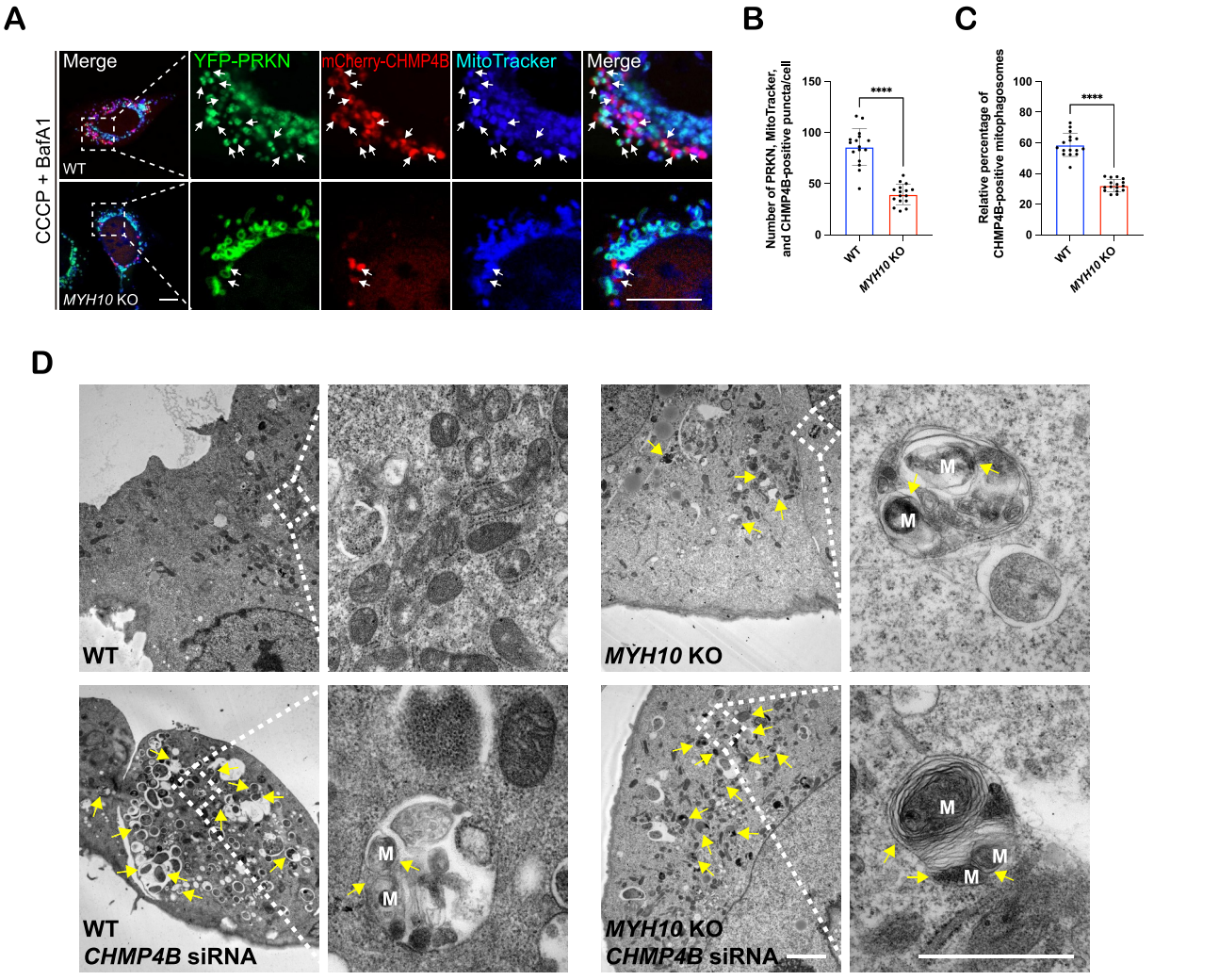

Figure 8. MYH10 recruits ESCRT-III to PRKN-positive damaged mitochondria to mediate mitophagosome sealing. (A) U2OS cells stably expressing YFP-PRKN and mCherry-CHMP4B were stained with MitoTracker (blue) and treated with carbonyl cyanide m-chlorophenyl hydrazone (CCCP, 20 μM) and bafilomycin A_1 (BafA1, 100 nM) for 2 h. White arrows indicate PRKN- and CHMP4B-positive mitochondria. Scale bar: 20 μm. (B-C) Number and relative percentage of PRKN- and CHMP4B-positive mitophagosomes, which was calculated as the number of CHMP4B-positive mitophagosomes divided by the total number of PRKN-positive damaged mitochondria. Values are mean ± SEM of $n > 16$ randomly selected cells. $^{*}P < 0.05$, $^{**}P < 0.01$, $^{***}P < 0.001$, $^{****}P < 0.0001$ by paired two-tailed t test. (D) Representative transmission electron microscopy (TEM) images of mitochondria-containing multilamellar structures in WT or *MYH10* KO U2OS cells. The cells were treated with CCCP (20 μM) for 2 h in the absence or presence of *CHMP4B* knockdown. Yellow arrows indicate multilamellar structures; M indicates mitochondria. Scale bar: 2 μm.

associated mutant CHMP2B and that MYH10 participates in induced but not basal autophagy by binding to and recruiting autophagic receptor proteins. More importantly, MYH10 interacted with ESCRT-III to regulate autophagosome maturation by recruiting ESCRT-III to damaged mitochondria. Thus, MYH10 has a dual role in the activation of induced autophagy and in ESCRT-III-mediated phagophore closure, revealing novel functions of MYH10 in the autophagy pathway and ESCRT-related FTD pathogenesis.

One of the most imperative findings of the current study is that MYH10 participates in autophagosome closure. Four lines of evidence support this finding. First, the C-terminus of MYH10 interacts with CHMP4B and CHMP2B, two subunits of ESCRT-III, which participate in autophagosome sealing [21–23,25,26]. Second, the percentage of STX17-positive vesicles among all LC3-II-positive autophagosomes is decreased in *MYH10* KO cells, suggesting that MYH10 contributes to autophagosome maturation. Third, MYH10 recruits ESCRT-III to PRKN-positive mitochondria damaged by CCCP treatment, indicating that myosin IIB links ESCRT-III to unsealed phagophores to mediate membrane closure. Fourth, *MYH10* KO cells resulted in the accumulation of multilamellar structures containing damaged mitochondria after CCCP treatment, a cellular phenotype identical to that of *CHMP4B* knockdown. Thus, MYH10, like CHMP4B, is required for mitophagosome closure. Without MYH10 or CHMP4B activity, mitophagosomes fail to seal and their membranes continue to grow and form multilamellar structures. Thus, MYH10 is an important novel player in the molecular machinery required for autophagosome closure.

We also found that MYH10 plays a role in the early activation of induced but not basal autophagy, adding to growing evidence that the myosin family is involved in different steps of autophagy. To expand, it is reported that MYH9 interacts with ATG9A and regulates its trafficking from the trans-Golgi network to the autophagosome initiation site [5]. In contrast, MYH6 delivers endosomal membranes by binding to Tom1 to facilitate autophagosome-lysosome fusion [6]; this step in the autophagy pathway is also influenced indirectly by MYO1C, a motor protein required for lipid raft trafficking [7]. Since autophagy is highly regulated, much remains to be learned about how autophagic membrane components and cargos are assembled and transported inside the cell.

Our study also identified *MYH10* as a strong novel genetic suppressor of the toxicity of FTD-associated mutant CHMP2B. We found that partial knockdown of *MYH10* rescues the toxicity caused by the accumulation of abnormal autophagosomes induced by mutant CHMP2B, consistent with our previous finding that *Atg5* knockdown also suppresses the toxicity of mutant CHMP2B in neurons [16]. Lysosome dysfunction or blockage of autophagosome–lysosome fusion is common in neurodegenerative diseases [8]. Thus, it is very important to fully understand the exact defects at different steps of autophagy in a specific disease. MYH10 or other proteins that promote autophagy induction may serve as therapeutic targets for neurodegenerative conditions in which autophagosome accumulation contributes to disease pathogenesis.

Materials and methods

Cell culture

Human bone osteosarcoma epithelial cells (U2OS) and HEK293T cell lines were purchased from the American Type Culture Collection (ATCC, HTB-96 and CRL-11268) and maintained in Dulbecco's Modified Eagle's Medium (DMEM; Corning, 10–013-CV) supplemented with 10% (v:v) fetal bovine serum (FBS; Thermo Fisher Scientific, 10–437-028) and penicillin-streptomycin (Gibco, 15140122) in a humidified atmosphere with 5% (v:v) CO_2 at 37°C.

Transfections

Cells were transiently transfected with 10 μM siRNA using Lipofectamine RNAiMAX (Invitrogen, 13778075) and/or plasmid DNA using Lipofectamine 3000 (Invitrogen, L3000015) according to the manufacturer's instructions. At 24–48 h after transfection, cells were processed for the corresponding assay, and the efficiency of protein depletion was assessed by Western blotting.

Generation of MYH10 KO cell lines

MYH10 KO cells were generated using RNA-guided CRISPR-Cas9. Cells were transfected with guide RNAs encoding pSpCas9(BB)-2A-puro plasmids (Addgene, 62988). Transfected cells were selected with 1 μg/ml puromycin (Thermo Scientific, A1113803) for 4–5 days. The resulting clonal cell colonies were expanded and characterized by western blotting and genome sequencing.

Immunoprecipitations

Cells were lysed with lysis buffer (50 mM Tris-HCl, pH 7.6, 150 mM NaCl, 2 mM EDTA, 1% NP-40 [Thermo Scientific, 85124] or 1% Triton X-100 [Promega, H5141]) supplemented with protease and phosphatase inhibitor (Thermo Scientific, 78442) on ice for 30 min and centrifuged at 16,000 *g* at 4°C for 15 min. The supernatants were incubated with primary antibodies at 4°C overnight. Subsequently, the protein G PLUS-agarose beads (Santa Cruz Biotechnology, sc-2002) were washed three times with lysis buffer. If required, the immunoprecipitated proteins were eluted by adding 2 μg/ml of FLAG peptides (Sigma, F4799-4mg). Immunoprecipitated proteins were separated by SDS-PAGE and analyzed by immunoblotting.

Immunoblotting

The cultured cells and iPSC-derived cortical neurons were washed with PBS (Corning, 21–031-CV) prior to lysis. The cell lysates were prepared using RIPA buffer (Thermo Scientific, 89901) supplemented with protease and phosphatase inhibitor (Thermo Scientific, 78442), and were incubated for 30 min on ice. Crude RIPA lysates were centrifuged at 14,000 g for 15 min at 4°C to remove cellular debris. The remaining supernatant was transferred to a new tube and quantified with a Pierce BCA protein assay (Thermo Scientific, 23227). Cell lysates were mixed with Laemmli Sample Buffer (Bio-Rad, 1610747) with beta-mercaptoethanol (Sigma, M3148-100ML) and incubated for 10 min at 95°C. Equal amounts of protein were subjected to SDS–PAGE, transferred to PVDF Membrane (Millipore, IPFL00010) using Trans-Blot Turbo Transfer device (Bio-Rad, 1704150). Membranes were blocked with Odyssey PBS Blocking Buffers (LI-COR Biosciences, 927–40010) at room temperature for 1 h and treated over night at 4°C with primary antibodies listed in Table 1. Following incubation overnight, horseradish peroxidase-conjugated secondary antibodies listed in Table 1 and WesternBright ECL Kit (Advansta, K-12045-D50) were used to detect protein signals. Protein bands were quantified using Fiji software (NIH). For the fluorescent western images, after primary antibody incubation, the membranes were washed with TBST (Thermo Scientific, 28360) and incubated with IRDye secondary antibodies listed in Table 1 and images were acquired with the iBright FL1500 Imaging System (Thermo Scientific, 927-A44241).

Immunofluorescence

U2OS cells and iPSC-derived cortical neurons were grown on Poly-D-Lysine/Laminin Coated glass coverslips (Thermo Scientific, 354087 or Corning, 354087) in multi-well cell culture plates (TTE Laboratories, CT2203) and were stained through standard immunocytochemistry

Table 1. Reagents and resources used in this study.

Reagent or Resource		
Antibodies	**Source**	**Identifier (Cat#, Antibody ID)**
Mouse anti-Flag	Sigma-Aldrich	F1804, RRID:AB_262044
Mouse anti-Flag Magnetic	Sigma-Aldrich	M8823, RRID:AB_2637089
Mouse anti-Flag Affinity Gel	Sigma-Aldrich	A2220, RRID:AB_10063035
Mouse anti-ACTB/β-actin	Santa Cruz Biotechnology	sc-47778, RRID:AB_2714189
Rabbit anti-ACTB	Cell Signaling Technology	4970, RRID:AB_2223172
Rabbit anti-CHMP4B	Proteintech	13683-1-AP, RRID:AB_2877971
Rabbit anti-MYH10/myosin IIB	BioLegend	909901, RRID:AB_2565101
Rabbit anti-MYH10	Sigma-Aldrich	M7939, RRID:AB_260669
Rabbit anti-MYO5B/myosin VB	Novus	NBP1-87746, RRID:AB_11034537
Mouse anti-GFP	Santa Cruz Biotechnology	sc-9996, RRID:AB_627695
Mouse anti-MYC/c-Myc	Santa Cruz Biotechnology	sc-40, RRID:AB_627268
Mouse anti-SQSTM1/p62	Sigma-Aldrich	WH0008878M1, RRID:AB_1843748
Pig anti-SQSTM1	Progen	GSQSTM1-C, RRID:AB_2687531
Rabbit anti-LC3	Sigma-Aldrich	L7543, RRID:AB_796155
Rabbit anti-LC3	Novus	NB100-2220, RRID:AB_10003146
Rabbit anti-LC3	MBL International	PM036, RRID:AB_2274121
Mouse anti-LC3	MBL International	M152-3, RRID:AB_1279144
Mouse anti-LC3	Cosmo Bio	CAC-CTB-LC3-2-IC, RRID:AB_10707197
Rabbit anti-CANX/Calnexin	Abcam	ab22595, RRID:AB_2069006
Rabbit anti-OPTN	Abcam	ab23666, RRID:AB_447598
Rabbit anti-mCherry	Abcam	ab167453, RRID:AB_2571870
Protein G PLUS-Agarose	Santa Cruz Biotechnology	sc-2002, RRID:AB_10200697
Goat anti-Mouse IgG, Alexa Fluor 405	Thermo Fisher Scientific	A-31553, RRID:AB_221604
Goat anti-Rabbit IgG, Alexa Fluor 405	Thermo Fisher Scientific	A-31556, RRID:AB_221605
Donkey anti-Mouse IgG, Alexa Fluor 488	Thermo Fisher Scientific	A-21202, RRID:AB_141607
Goat anti-Rabbit IgG, Alexa Fluor 488	Thermo Fisher Scientific	A-11008, RRID:AB_143165
Donkey anti-Rabbit IgG, Alexa Fluor 488	Thermo Fisher Scientific	A-21206, RRID:AB_2535792
Goat anti-Mouse IgG, Alexa Fluor 568	Thermo Fisher Scientific	A-11004, RRID:AB_2534072
Donkey anti-Rabbit IgG, Alexa Fluor 568	Thermo Fisher Scientific	A10042, RRID:AB_2534017
IRDye® 800CW Donkey anti-Mouse IgG	LI-COR Biosciences	926–32212, RRID:AB_621847
IRDye® 800CW Donkey anti-Rabbit IgG	LI-COR Biosciences	926–32213, RRID:AB_621848
IRDye® 680CW Donkey anti-Mouse IgG	LI-COR Biosciences	926–68070, RRID:AB_10956588
IRDye® 680CW Donkey anti-Rabbit IgG	LI-COR Biosciences	926–68071, RRID:AB_10956166
donkey anti-rabbit IgG-HRP: sc-2313	Santa Cruz Biotechnology	sc-2313, RRID:AB_641181
goat anti-mouse IgG-HRP: sc-2005	Santa Cruz Biotechnology	sc-2005, RRID:AB_631736
Chemicals	**SOURCE**	**Cat.**
Puromycin dihydrochloride	Thermo Fisher Scientific Gibco	A1113803
Blasticidin S HCl (10 mg/mL)	Thermo Fisher Scientific Gibco	A1113903
3X Flag® Peptide	Sigma-Aldrich	F4799-4mg
Lipofectamine RNAiMAX	Thermo Fisher Scientific	13778075
Lipofectamine 3000	Thermo Fisher Scientific	L3000015
Halt Protease and Phosphatase Inhibitor Cocktail, EDTA-free (100X)	Thermo Fisher Scientific	78442
Protease/Phosphatase Inhibitor Cocktail (100X)	Cell Signaling Technology	5872S
cOmplete™, Mini, EDTA-free Protease Inhibitor Cocktail	Roche	11836170001
Thermo Scientific Pierce RIPA Buffer	Thermo Fisher Scientific	89901
Paraformaldehyde Solution, 4% in PBS, Thermo Scientific™	Thermo Fisher Scientific	AAJ19943K2
16% Paraformaldehyde (Formaldehyde) Aqueous Solution	Electron Microscopy Sciences	15710-S
MitoTracker™ Red CMXRos	Thermo Fisher Scientific Invitrogen	M7512
BioTracker MitoBlue Live Cell Dye	MilliporeSigma	SCT086
D-MEM (high glucose) with sodium pyruvate, without Amino Acids	FUJIFILM Wako Pure Chemical Corporation	048–33575
Bafilomycin A1	Santa Cruz Biotechnology	sc-201550
CCCP, mitochondrial oxidative phosphorylation uncoupler	Abcam	ab141229
PageSilver Silver Staining Kit	Thermo Fisher Scientific	K0681
WesternBright ECL Kit	Advansta	K-12045-D50
Experimental Models: Cell Lines	**SOURCE**	**Cat.**
HEK293T	ATCC	CRL-11268
U2OS	ATCC	HTB-96
U2OS (*MYH10* KO)	This study	N.A.
Normal iPSC (24#2)	This study	N.A.
Normal iPSC (35#11)	This study	N.A.
Oligonucleotides	**Use**	**Backbone vector (reference) and restriction enzyme(s)**
Negative Control siRNA		Qiagen, 1022076
FlexiTube GeneSolution for *CHMP4B* (siRNA)		Qiagen, GS128866
MYH10 KO sgRNA #1-F: 5′-CACCGAGGTATCTCTTTGTGGACA-3′ *MYH10* KO sgRNA #1-R: 5′-AAACTGTCCACAAAGAGATACCTC-3′	subcloning of sgRNA#1	pSpCas9(BB)-2A-puro (Addgene 62988; deposited by Feng Zhang) with BbsI
MYH10 KO sgRNA #2-F: 5′-CACCGTACTAGCTGCCTCAAAACCA-3′ *MYH10* KO sgRNA #2-R: 5′-AAACTGGTTTTGAGGCAGCTAGTAC-3′	subcloning of sgRNA#2+ A68:B68	pSpCas9(BB)-2A-Puro (Addgene 62988; deposited by Feng Zhang) with BbsI

(*Continued*)

Table 1. (Continued).

MYH10-F: 5′-ATAAGAATgcggccgcGatggcgcagagaactggact -3′ MYH10-R: 5′-GACGGTACCttactctgactggggtggct-3′	subcloning of Flag-MYH10	p3xFlag-CMV™-7.1 (Sigma, E7533) with NotI and KpnI
CHMP4B-F: 5′-GAAGATCTaatgtcggtgttcgggaag-3′ CHMP4B-R: 5′-CACGCGTCGACttacatggatccagccca-3′	subcloning of Flag-CHMP4B	p3xFlag-CMV™-7.1 (Sigma, E7533) with BglII and SalI
CHMP2B-F: 5′-TGACAAGCTTGCGGCCGCGatggcgtccctcttcaag-3′ CHMP2B-R: 5′-GATCCTCTAGActaatctactcctaaagc-3′	subcloning of Flag-CHMP2B	p3xFlag-CMV™-7.1 (Sigma, E7533) with NotI and XbaI
CHMP4B N-terminal fragment-F: 5′-GAAGATCTaatgtcggtgttcgggaag-3′ CHMP4B N-terminal fragment-R: 5′-CACGCGTCGACcgccttcatggccttggc-3′	subcloning of Flag-N half of CHMP4B	p3xFlag-CMV™-7.1 (Sigma, E7533) with BglII and SalI
CHMP4B C-terminal fragment-F: 5′-GAAGATCTagcccatgacaacatggac-3′ CHMP4B C-terminal fragment-R: 5′-CACGCGTCGACttacatggatccagccca-3′	subcloning of Flag-C half of CHMP4B	p3xFlag-CMV™-7.1 (Sigma, E7533) with BglII and SalI
M1-F: 5′-ATGCGGCCGCATGGCGCAGAGAACTGGA-3′ M1-R: 5′-ATGGTACCCCGGGGAGTCAGGATGGC-3′	subcloning of M1-MYC/cMyc	pcDNA3.1 myc-His (Invitrogen, V80020) with NotI and KpnI
M2-F: 5′-ATGCGGCCGCCGGCACTGGCAGTGGTGG-3′ M2-R: 5′-TCGGTACCCTCCAGGCCCTGCTTGTT-3′	subcloning of M2-MYC	pcDNA3.1 myc-His (Invitrogen, V80020) with NotI and KpnI
M3-F: 5′-ACGCGGCCGCGAAACTAAGAACCATGAA-3′ M3-R: 5′-ATGGTACCTTTCTTTGAAGCTACAGC-3′	subcloning of M3-MYC	pcDNA3.1 myc-His (Invitrogen, V80020) with NotI and KpnI
M4-F: 5′-ATGCGGCCGCAAAAAGATGGAGATAGAC-3′ M4-R: 5′-ATGGTACCCTCTGACTGGGGTGGCTG-3′	subcloning of M4-MYC	pcDNA3.1 myc-His (Invitrogen, V80020) with NotI and KpnI
N half of M4-F: 5′-ATGCGGCCGCAAAAAGATGGAGATAGAC -3′ N half of M4-R: 5′-TAGGTACCACCCTCGAGTTCCTGCAG-3	subcloning of N half of M4-MYC	pcDNA3.1 myc-His (Invitrogen, V80020) with NotI and KpnI
C half of M4-F: 5′-ACGCGGCCGCAAGCTGCAGGAACTCGAG -3′ C half of M4-R: 5′-ATGGTACCCTCTGACTGGGGTGGCTG-3′	subcloning of C half of M4-MYC	pcDNA3.1 myc-His (Invitrogen, V80020) with NotI and KpnI
CHMP4A-F: 5′-AAGCTTCGAATTCAATGTCGCGGCGGCGCCCT -3′ CHMP4A-R: 5′-CACGCGTCGACtcaggatacccactcagc-3′	subcloning of GFP-CHMP4A	pEGFP-C1 (Clontech, V012024) with EcoRI and SalI
CHMP2B^{intron5}-F: 5′-CACGCGTCGACatggcgtccctcttcaagaag -3′ CHMP2B^{intron5}-R: 5′-GTAGGGCCCctatacctttccagaaatttcaattcc-3′	subcloning of GFP-CHMP2B^{intron5}	pEGFP-C1 (Clontech, V012024) with SalI and ApaI
mRFP-F: 5′-TCAGATCCGCTAGCGCCACCatggcctcctccgaggac -3′ mRFP-R: 5′-GAATTCGAAGCTTGggcgccggtggagtggcg-3′	subcloning of pmRFP-C1	pEGFP-C1 (Clontech, V012024) with NheI and HindIII
CHMP4A-F: 5′-AAGCTTCGAATTCAATGTCGCGGCGGCGCCCT -3′ CHMP4A-R: 5′-CACGCGTCGACtcaggatacccactcagc-3′	subcloning of mRFP-CHMP4A	pmRFP-C1 with EcoRI and SalI
CMV-GFP-MYH10-F: 5′-gtgtatCATATGCCAAGTACG-3′ CMV-GFP-MYH10-R: 5′-gatgaattcgcggccgcttactctgactggggtgg-3′	subcloning of pLVX-Puro-GFP-MYH10	pLVX-Puro (Clontech, 632164) with NdeI and Not1
CMV-YFP-PRKN/parkin-F: 5′-gtgtatCATATGCCAAGTACG-3′ CMV-YFP-PRKN/parkin-R: 5′-atccggtggatccttacacgtcgaaccagtg-3′	subcloning of pLVX-Puro-YFP-PRKN /parkin	pLVX-Puro (Clontech, 632164) with NdeI and KpnI
mCherry-F: 5′-CTAGGGCTAGCGGATCCgtcgccaccatggtgagcaa-3′ mCherry-R: 5′-GCAGAATTCccggacttgtacagctcgtc-3′	subcloning of pLV-EF1a-Blast-mCherry	pLV-EF1a-IRES-Blast (Addgene, 85133; deposited by Tobias Meyer) with BamHI and EcoRI
CHMP4B-F: 5′-tccgggaattcATCGATAGATCTAatgtcg-3′ CHMP4B-R: 5′-ATAAGAATGCGGCCGCttacatggatccagcccagtt-3′	subcloning of pLV-EF1a-Blast-mCherry -CHMP4B	pLV-EF1a-IRES-Blast (Addgene, 85133; deposited by Tobias Meyer) with EcoRI and NotI
CHMP2B-F: 5′-ggaattcctcgaggGCGGCCGCGatggcgtccc-3′ CHMP2B-R: 5′-ccgtcgacTCTAGActaatctactcctaaagc-3′	subcloning of pLV-EF1a-Blast-mCherry -CHMP2B	pLV-EF1a-IRES-Blast (Addgene, 85133; deposited by Tobias Meyer) with NotI and XbaI
CHMP2B^{intron5}-F: 5′-cctcgaggGCGGCCGCGAATTCATCGATAGATCTGa-3′ CHMP2B^{intron5}-R: 5′-ccgtcgacTCTAGActaatctactcctaaagc-3′	subcloning of pLV-EF1a-Blast-mCherry -CHMP2B^{intron5}	pLV-EF1a-IRES-Blast (Addgene, 85133; deposited by Tobias Meyer) with NotI and XbaI
CMV-mCherry-PRKN/parkin-F: 5′-ccagtttatcgataagcttgggagttccgcgtt-3′ CMV-mCherry-PRKN/parkin-R: 5′-gcggccgcggatccttacacgtcgaaccagtg-3′	subcloning of pLV-CMV-Blast-mCherry -PRKN/parkin	pLV-EF1a-IRES-Blast (Addgene, 85133; deposited by Tobias Meyer) with ClaI and BamHI
mRFP-STX17/syntaxin 17-F: 5′-ccagtttatcgataagcttgggagttccgcgtt-3′ mRFP-STX17/syntaxin 17-R: 5′-tctagagcggccgcTCGAGGGATCCTTAACTGCATTTCT-3′	subcloning of pLV-CMV-Blast-mRFP-STX17/syntaxin 17	pLV-EF1a-IRES-Blast (Addgene, 85133; deposited by Tobias Meyer) with ClaI and NotI

Recombinant DNA	**Reference**	**Cat.**
p3xFlag-CMV™-7.1 Expression Vector	Sigma-Aldrich	E7533
p3xFlag-MYH10	This study	N.A.
p3xFlag-CHMP4B	This study	N.A.
p3xFlag-CHMP2B	This study	N.A.
p3xFlag-N half of CHMP4B	This study	N.A.
p3xFlag-C half of CHMP4B	This study	N.A.

(*Continued*)

Table 1. (Continued).

M1 of MYH10-cMc	This study	N.A.
M2 of MYH10-cMc	This study	N.A.
M3 of MYH10-cMc	This study	N.A.
M4 of MYH10-cMc	This study	N.A.
N half of M4 of MYH10-cMc	This study	N.A.
C half of M4 of MYH10-cMc	This study	N.A.
pEGFP-C1 vector	Clontech	V012024
pEGFP C1-CHMP4A	This study	N.A.
pEGFP C1-CHMP4B	Sino Biological	HG14022-ANG
pEGFP C1-CHMP4C	Sino Biological	HG14241-ANG
pEGFP C1-CHMP2B	Sino Biological	HG14596-ANG
pEGFP C1-CHMP2B^{intron5}	Sino Biological	N.A.
pEGFP-C3 vector	Clontech	V012022
pEGFP C3-MYH10	Addgene	11348; deposited by Robert Adelstein
GFP-OPTN	Sino Biological	HG14478-ANG
GFP-CALCOCO2/NDP52	Sino Biological	HG11425-ANG
GFP-SQSTM1	Sino Biological	HG17112-ANG
pmRFP C1	This study	N.A.
pmRFP C1-CHMP4A	This study	N.A.
pmRFP C1-CHMP4B	Sino Biological	HG14022-ANR
pmRFP C1-CHMP4C	Sino Biological	HG14241-ANR
mRFP-OPTN	Sino Biological	HG14478-ANR
mRFP-CALCOCO2/NDP52	Sino Biological	HG11425-ANR
mRFP-SQSTM1	Sino Biological	HG17112-ANR
pLVX-Puro Vector Information	Clontech	632164
pLVX-Puro-GFP-MYH10	This study	N.A.
pLVX-Puro-YFP-PRKN/parkin	This study	N.A.
pLV-EF1a-Blast	Addgene	85133; deposited by Tobias Meyer
pLV-EF1a-Blast-mCherry	This study	N.A.
pLV-EF1a-Blast-mCherry-CHMP2B	This study	N.A.
pLV-EF1a-Blast-mCherry-CHMP2B^{intron5}	This study	N.A.
pLV-CMV-Blast-mCherry-PRKN/parkin	This study	N.A.
pLV-CMV-Blast-mRFP-STX17/syntaxin 17	This study	N.A.
TRC Lentiviral pLKO.1 empty vector	RNAi Core Facility in UMass	RHS4080
TRC Lentiviral *MYH10* shRNA#1	RNAi Core Facility in UMass	TRCN0000123074
TRC Lentiviral *MYH10* shRNA#2	RNAi Core Facility in UMass	TRCN0000123078

techniques. Briefly, cells were fixed with 4% paraformaldehyde (Thermo Scientific, AAJ19943K2) for 10 min at room temperature. Fixed cells were rinsed 3 times with PBS and permeabilized using 50 μg/ml digitonin (Sigma, D141-100mg) in PBS for 5 min at room temperature. The cells were then washed with PBS, blocked with 3% BSA (Sigma, A7906-100g) for 30 min at room temperature. After primary antibody incubation listed in Table 1 for 1 h at room temperature, cells were rinsed with PBS. Cells were incubated with fluorescently labeled secondary antibodies listed in Table 1 for 1 h at room temperature, and stained with DNA labeling Hoechst (Thermo Scientific, H3569) for 20 min at room temperature. Images were acquired with a laser-scanning confocal microscope (Carl Zeiss, LSM 800).

DNA constructs

A list of relevant plasmids and oligonucleotides is provided in Table 1. To generate recombinant DNA, the DNA fragments were amplified by PCR using specific primers and inserted into specific backbone vectors with restriction enzymes (see Table 1).

Cortical neuron differentiation

Human iPSCs were differentiated into cortical neurons as described [33] with some modifications. Briefly, iPSCs were expanded in Matrigel-coated wells (Corning, 354230) and at 60% confluency were split with Accutase (EMD Millipore, SCR005) and placed in Matrigel-coated wells. The next day, the culture medium was replaced with neuroepithelial progenitor (NEP) medium (DMEM/F12 [Gibco, 12660012], neurobasal medium [Gibco, 21103049] at 1:1, 0.5X N2 supplement [Gibco, 17502048], 0.5X B27 supplement [Gibco, 17504044], 0.1 mM Ascorbic Acid [Sigma, A4403-100mg], 1X Glutamax [Gibco, 35050061], 3 μM CHIR99021 [Stem Cell Technologies, 72054], 2 μM DMH1 [Stem Cell Technologies, 73634], and 2 μM SB431542 [Stemgent, 04–0010-10]) for 6 days. NEPs were dissociated with Accutase and split 1:6 into Matrigel-coated wells. NEPs were cultured in neuron progenitor induction NPI medium (DMEM/F12, neurobasal medium at 1:1, 0.5X N2 supplement, 0.5X B27 supplement, 0.1 mM Ascorbic Acid, 1X Glutamax, 1.02 μM CHIR99021, 2 μM DMH1, 2 μM SB431542, and 2 μM Cyclopamine [Stem Cell Technologies, 72074]) for 6 days. The cells were dissociated with Accutase and split into culture dishes (Corning, 3261) to generate suspension cultures. The cells were cultured in neuron A medium (DMEM/F12, neurobasal medium at 1:1, 0.5X N2 supplement, 0.5X B27 supplement, 0.1 mM Ascorbic Acid, and 1X Glutamax) for 6 days. Finally, the cells were dissociated into single cells and plated on Poly-D-Lysine/Laminin Coated glass coverslips (Corning, 354087) in neuron B medium (DMEM/F12, neurobasal medium at 1:1, 0.5X N2 supplement, 0.5X B27 supplement, 0.1 mM Ascorbic Acid, and 1X Glutamax, 0.1 μM Compound E [Stem Cell Technologies, 73954], 1 μg/ml

Laminin [Sigma, L2020], 10 ng/ml GDNF [R&D Systems, 212-GD-050] and 10 ng/ml BDNF [R&D Systems, 248-BDB -050]) for up to 1–3 months.

Lentivirus production and infection

The lentiviral shRNA clones targeting *MYH10* (TRCN0000123074 and TRCN0000123078) were purchased from RNAi Core Facility at the University of Massachusetts Chan Medical School. Lentiviruses, including shRNAs and expression vectors, were produced following published protocols [49]. For stable cell lines, the U2OS cells were infected with the virus for 24 h. The medium was replaced with fresh medium, and the cells were treated with puromycin (2 μg/ml) or blasticidin (2 μg/ml) for 24 h and then maintained in medium containing puromycin (1 μg/ml) or blasticidin (1 μg/ml). Selected U2OS cells were grown in antibiotic-free medium for 24 h before experiments.

Transmission electron microscopy

U2OS cells were cultured in Dulbecco's Modified Eagle's Medium supplemented with 10% (v:v) fetal bovine serum and 1% penicillin-streptomycin in an incubator with 5% CO_2 at 37°C. Plated U2OS cells were treated with CCCP (20 μM; Abcam, ab141229) for 2 h in the absence or presence of *CHMP4B* knockdown and were fixed by first removing half the plate media and then adding equal volume of 2.5% glutaraldehyde (v:v) in 1 M sodium cacodylate buffer (pH 7.2) to each of the wells in the culture plate and allowed to fixed for 10 min before being transferred to pure 2.5% glutaraldehyde (v:v) in 1 M sodium cacodylate buffer (pH 7.2) for 1 h. Next the cell plates were briefly rinsed (3x10 min) in 1 M sodium cacodylate buffer (pH 7.2) and post-fixed for 1 h in 1% osmium tetroxide (w:v) in dH_2O. Samples were then washed three times with dH_2O for 10 mins and then cells were scraped off the bottom of the wells with a soft plastic spatula, collected in a microfuge tube, and pelleted by centrifugation. Samples were washed three times with dH_2O for 10 min and dehydrated through a graded series of ethanol (10, 30, 50, 70, 85, 95% for 20 min each) to three changes of 100% ethanol. Samples were infiltrated first with two changes of 100% propylene oxide (SPI Supplies, 75–56-9 [02659-AB]) and then with a 50%:50% propylene oxide:SPI-Pon 812 resin (SPI Supplies, 90529–77-4 [02659-AB], 26544–38-7 [02827-AF], 25068–38-6;84–74-2 [02816-AB], and 90–72-2 [02823-DA]) mixture overnight.

The following morning the cell pellets were transferred through four changes of fresh SPIpon 812- Araldite epoxy resin and finally embedded in tubes filled with the same resin and polymerized for 48 h at 70°C. The epoxy blocks were then trimmed, and ultrathin sections were cut on a Reichart-Jung ultramicrotome using a diamond knife. The sections were collected and mounted on copper support grids and contrasted with lead citrate and uranyl acetate. The samples were examined on a Philips CM 10 using 100 Kv accelerating voltage. Images were captured using a Gatan TEM CCD camera.

Drosophila *strains*

Flies were maintained on a standard yeast diet at 25°C in an incubator. w^{1118} was used as a wild-type control. w^{1118}, *GMR-Gal4*, UAS-mCherry RNAi (BL35785), *zip* RNAi#1 (BL37480), *zip* RNAi#2 (v7819), and a zip^{1} null mutant (BL4199), and RNAi lines were from the Bloomington *Drosophila* Stock Center or the Vienna *Drosophila* Resource Center. *GMR-Gal4, UAS-CHMP2B*^{intron5} and *GMR-Gal4, UAS-CHMP2B*^{WT} recombinant flies were generated previously [29].

Drosophila *eye morphological defects analysis*

Flies for analysis of eye phenotype were crossed and raised at 27°C to promote CHMP2B^{intron5} expression. Flies of all genotypes were collected and aged for ~10 days. Adult flies (10 days old) were examined with a dissecting microscope (Nikon, SMZ 1500), and the severity of eye morphological defects (e.g., loss of pigmentation and rough eye) were classified as low, medium, or high. Each group of flies was quantified by category, and the data were analyzed by chi-square test. Both male and female flies were used for all experiments.

RNA extraction and real-time quantitative PCR

Forty fly heads were collected into a 1.5 ml tube and frozen in liquid nitrogen. Total RNA was extracted with Trizol (Qiagen, 79306) and the RNeasy Mini Kit (Qiagen, 74106), and 1 μg of RNA of each sample was then reverse transcribed to cDNA with the TaqMan Reverse Transcription Kit (Thermo Scientific, N8080234). Quantitative real-time PCR was done with SYBR Select Master Mix (Thermo Scientific, 4472918) on a QuantStudio 3 System. The primers used were *Drosophila zip* (forward: 5′-ACTGCTGGATGAGGAGTGCT-3′ and reverse: 5′-ACTTGGGGTGCATAGAGTGG-3′) and *Actin42A* (forward: 5′-TCTTACTGAGCGCGGTTACAG-3′ and reverse: 5′-ATGTCGCGCACAATTTCAC-3′). Ct values for each gene were normalized to internal controls as indicated. Relative mRNA expression was calculated with the delta-delta Ct method.

Statistical analysis

Statistical analyses were performed with chi-square test, paired two-tailed *t* test, one-way ANOVA with Tukey post-hoc test, or two-way ANOVA followed by Tukey's post hoc test for multiple comparisons with an appropriate test using GraphPad Prism version 9.0.0 software. Statistical significance was assumed with $^{*}P < 0.05$, $^{**}P < 0.01$, $^{***}P < 0.001$, $^{****}P < 0.0001$. The data are presented as mean ± standard error of the mean (SEM).

Acknowledgments

We thank the UMass Chan Medical School Electron Microscopy and Digital Imaging Cores for assistance, the Bloomington *Drosophila* Stock Center, and the Vienna *Drosophila* Resource Center for fly lines. Several figures were partially created with BioRender.com.

Disclosure statement

No potential conflict of interest was reported by the authors.

Funding

This work was supported by the National Institutes of Health (R37NS057553 and R01NS101986 to F.-B.G.), Basic Science Research Program through the National Research Foundation of Korea (NRF) funded by the Ministry of Education (NRF-2019R1A6A3A03034014 to Y.-W.J.), the Korean National Research Foundation (NRF-2020R1A2C2005021 to J.L.) and Science Research Center Program (2020R1A5A1019023 to J.L.).

References

[1] Mizushima N, Levine B, Cuervo AM, et al. Autophagy fights disease through cellular self-digestion. Nature. 2008;451:1069–1075.
[2] Galluzzi L, Baehrecke EH, Ballabio A, et al. Molecular definitions of autophagy and related processes. Embo J. 2017;36:1811–1836.
[3] Hosokawa N, Hara T, Kaizuka T, et al. Nutrient-dependent mTORC1 association with the ULK1-Atg13-FIP200 complex required for autophagy. Mol Biol Cell. 2009;20:1981–1991.
[4] Jung CH, Jun CB, Ro SH, et al. ULK-Atg13-FIP200 complexes mediate mTOR signaling to the autophagy machinery. Mol Biol Cell. 2009;20:1992–2003.
[5] Tang HW, Wang YB, Wang SL, et al. Atg1-mediated myosin II activation regulates autophagosome formation during starvation-induced autophagy. Embo J. 2011;30:636–651.
[6] Tumbarello DA, Waxse BJ, Arden SD, et al. Autophagy receptors link myosin VI to autophagosomes to mediate Tom1-dependent autophagosome maturation and fusion with the lysosome. Nat Cell Biol. 2012;14:1024–1035.
[7] Brandstaetter H, Kishi-Itakura C, Tumbarello DA, et al. Loss of functional MYO1C/myosin 1c, a motor protein involved in lipid raft trafficking, disrupts autophagosome-lysosome fusion. Autophagy. 2014;10:2310–2323.
[8] Nixon RA. The role of autophagy in neurodegenerative disease. Nat Med. 2013;19:983–997.
[9] Fleming A, Bourdenx M, Fujimaki M, et al. The different autophagy degradation pathways and neurodegeneration. Neuron. 2022;110:935–966.
[10] Sellier C, Campanari ML, Julie Corbier C, et al. Loss of C9ORF72 impairs autophagy and synergizes with polyQ Ataxin-2 to induce motor neuron dysfunction and cell death. Embo J. 2016;35:1276–1297.
[11] Webster CP, Smith EF, Bauer CS, et al. The C9orf72 protein interacts with Rab1a and the ULK1 complex to regulate initiation of autophagy. Embo J. 2016;35:1656–1676.
[12] Jung J, Nayak A, Schaeffer V, et al. Multiplex image-based autophagy RNAi screening identifies SMCR8 as ULK1 kinase activity and gene expression regulator. Elife. 2017:6.
[13] Yang M, Liang C, Swaminathan K, et al. A C9ORF72/SMCR8-containing complex regulates ULK1 and plays a dual role in autophagy. Sci Adv. 2016;2:e1601167.
[14] Zhu Q, Jiang J, Gendron TF, et al. Reduced C9ORF72 function exacerbates gain of toxicity from ALS/FTD-causing repeat expansion in C9orf72. Nat Neurosci. 2020;23:615–624.
[15] Boivin M, Pfister V, Gaucherot A, et al. Reduced autophagy upon C9ORF72 loss synergizes with dipeptide repeat protein toxicity in G4C2 repeat expansion disorders. Embo J. 2020;39:e100574.
[16] Lee JA, Gao FB. Inhibition of autophagy induction delays neuronal cell loss caused by dysfunctional ESCRT-III in frontotemporal dementia. J Neurosci. 2009;29:8506–8511.
[17] Lee JA, Beigneux A, Ahmad ST, et al. ESCRT-III dysfunction causes autophagosome accumulation and neurodegeneration. Curr Biol. 2007;17:1561–1567.
[18] Rusten TE, Vaccari T, Lindmo K, et al. ESCRTs and Fab1 regulate distinct steps of autophagy. Curr Biol. 2007;17:1817–1825.
[19] Filimonenko M, Stuffers S, Raiborg C, et al. Functional multivesicular bodies are required for autophagic clearance of protein aggregates associated with neurodegenerative disease. J Cell Biol. 2007;179:485–500.
[20] Hurley JH, Hanson PI. Membrane budding and scission by the ESCRT machinery: it's all in the neck. Nat Rev Mol Cell Biol. 2010;11:556–566.
[21] Lu Y, Zhang Z, Sun D, et al. Syntaxin 13, a genetic modifier of mutant CHMP2B in frontotemporal dementia, is required for autophagosome maturation. Mol Cell. 2013;52:264–271.
[22] Takahashi Y, He H, Tang Z, et al. An autophagy assay reveals the ESCRT-III component CHMP2A as a regulator of phagophore closure. Nat Commun. 2018;9:2855.
[23] Zhou F, Wu Z, Zhao M, et al. Rab5-dependent autophagosome closure by ESCRT. J Cell Biol. 2019;218:1908–1927.
[24] Knorr RL, Lipowsky R, Dimova R. Autophagosome closure requires membrane scission. Autophagy. 2015;11:2134–2137.
[25] Vietri M, Radulovic M, Stenmark H. The many functions of ESCRTs. Nat Rev Mol Cell Biol. 2020;21:25–42.
[26] Chang C, Jensen LE, Hurley JH. Autophagosome biogenesis comes out of the black box. Nat Cell Biol. 2021;23:450–456.
[27] West RJ, Lu Y, Marie B, et al. Rab8, POSH, and TAK1 regulate synaptic growth in a Drosophila model of frontotemporal dementia. J Cell Biol. 2015;208:931–947.
[28] Lu Y, Almeida S, Gao FB. TBK1 haploinsufficiency in ALS and FTD compromises membrane trafficking. Acta Neuropathol. 2021;142:217–221.
[29] Ahmad ST, Sweeney ST, Lee JA, et al. Genetic screen identifies serpin5 as a regulator of the toll pathway and CHMP2B toxicity associated with frontotemporal dementia. Proc Natl Acad Sci U S A. 2009;106:12168–12173.
[30] Young PE, Richman AM, Ketchum AS, et al. Morphogenesis in Drosophila requires nonmuscle myosin heavy chain function. Genes Dev. 1993;7:29–41.
[31] Müsch A, Cohen D, Rodriguez-Boulan E. Myosin II is involved in the production of constitutive transport vesicles from the TGN. J Cell Biol. 1997;138:291–306.
[32] Jun MH, Jang JW, Jeon P, et al. Nonmuscle myosin IIB regulates Parkin-mediated mitophagy associated with amyotrophic lateral sclerosis-linked TDP-43. Cell Death Dis. 2020;11:952.
[33] Yuva-Aydemir Y, Almeida S, Krishnan G, et al. Transcription elongation factor AFF2/FMR2 regulates expression of expanded GGGGCC repeat-containing C9ORF72 allele in ALS/FTD. Nat Commun. 2019;10:5466.
[34] Ye X, Zhou XJ, Zhang H. Exploring the role of autophagy-related Gene 5 (ATG5) yields important insights into autophagy in autoimmune/autoinflammatory diseases. Front Immunol. 2018;9:2334.
[35] Wong YC, Holzbaur EL. Optineurin is an autophagy receptor for damaged mitochondria in parkin-mediated mitophagy that is disrupted by an ALS-linked mutation. Proc Natl Acad Sci U S A. 2014;111:E4439–48.
[36] Harding O, Evans CS, Ye J, et al. ALS-and FTD-associated missense mutations in TBK1 differentially disrupt mitophagy. Proc Natl Acad Sci U S A. 2021;118:e2025053118.
[37] Clark EH, Vázquez de la Torre A, Hoshikawa T, et al. Targeting mitophagy in Parkinson's disease. J Biol Chem. 2021;296:100209.
[38] Itakura E, Mizushima N. p62 targeting to the autophagosome formation site requires self-oligomerization but not LC3 binding. J Cell Biol. 2011;192:17–27.
[39] Mijaljica D, Nazarko TY, Brumell JH, et al. Receptor protein complexes are in control of autophagy. Autophagy. 2012;8:1701–1705.
[40] Rogov V, Dötsch V, Johansen T, et al. Interactions between autophagy receptors and ubiquitin-like proteins form the molecular basis for selective autophagy. Mol Cell. 2014;53:167–178.
[41] Kast DJ, Dominguez R. The cytoskeleton-autophagy connection. Curr Biol. 2017;27:R318–r26.

[42] Lee JA, Liu L, Javier R, et al. ESCRT-III subunits Snf7-1 and Snf7-2 differentially regulate transmembrane cargos in hESC-derived human neurons. Mol Brain. 2011;4:37.
[43] Zhen Y, Spangenberg H, Munson MJ, et al. ESCRT-mediated phagophore sealing during mitophagy. Autophagy. 2020;16:826–841.
[44] Muzioł T, Pineda-Molina E, Ravelli RB, et al. Structural basis for budding by the ESCRT-III factor CHMP3. Dev Cell. 2006;10:821–830.
[45] Lata S, Roessle M, Solomons J, et al. Structural basis for autoinhibition of ESCRT-III CHMP3. J Mol Biol. 2008;378:818–827.
[46] Obita T, Saksena S, Ghazi-Tabatabai S, et al. Structural basis for selective recognition of ESCRT-III by the AAA ATPase Vps4. Nature. 2007;449:735–739.
[47] McCullough J, Fisher RD, Whitby FG, et al. ALIX-CHMP4 interactions in the human ESCRT pathway. Proc Natl Acad Sci U S A. 2008;105:7687–7691.
[48] Tang S, Henne WM, Borbat PP, et al. Structural basis for activation, assembly and membrane binding of ESCRT-III Snf7 filaments. Elife. 2015;4:E4439–48.
[49] Tiscornia G, Singer O, Verma IM. Production and purification of lentiviral vectors. Nat Protoc. 2006;1:241–245.